Studies of Phase Transformations in Ti-Al-X Alloys

S.K.Sahay, S.K.Singh, B.Goswami and A.K.Ray*

National Institute of Technology, Jamshedpur, India
** National Metallurgical Laboratory, Jamshedpur, India*

ABSTRACT

Phase transformation in titanium alloys on high temperature exposure has been studied. The central theme of review includes the study of basic development in phase transformation, microstructural features, acceptability of crystalline modification, precipitation and intermetallics formation. Effects of alloying elements to the standard systems have been studied. Lamellar microstructure in titanium aluminide systems forms various typical fronts of microstructural changes, where equiax, duplex, ultra fine grained combinations in lamellar or other phases produce versatile implications to the scenario. Ti-6Al-4V systems have been referred to as the 'work horse' of component manufacturing in industry and airways. Twinning, an important deformation mechanism, arises from stress fields associated to misfitting interfacial dislocation or shear reshuffle. Mostly lamellar topography of these systems shows a better creep life after reduction of dislocation climb process by segregated solutes at ledges of lamella. Industrial, biomedical, airways, aerospace and electrical sensors industry are main component manufacturer from these different standard alloy systems.

Key words: Titanium aluminides, Intermetallics, Phase transformation, Stability, Lamellar, Precipitation, Twins, Martensite.

INTRODUCTION

A series of classical investigations on the study of phase transformations in Ti-Al-X systems led to a better understanding of the stability of phases. Intensive research has been done over the past two decades in order to enhance the ductility and fracture toughness at room temperature and oxidation, corrosion and creep resistance at elevated temperature in Ti-Al-X alloys. The study of phase transformation in Ti-Al-X alloys is interesting from a fundamental point of view, as it has enormous practical consequences. The development of Ti-Al-X alloys for high temperature applications is based on a solid technical foundation and triggered by economic considerations. Major developments in Ti-Al-X alloys have been stimulated through intensive research over the past two decades. The stringent requirements for high temperature applications of Ti-Al-X alloys have been met as our knowledge has increased of the kinetics, thermodynamics and mechanism of phase-transformations. The search for improved high temperature alloys will continue to take advantage of every last vestige of properties such as strengths, ductility, creep resistance, oxidation, corrosion, etc.

The advent of new experimental techniques such as TEM, STEM and electron probe microanalysis and related analytical techniques like EDX, etc., has made extensive contributions to enhance the understanding of the phase-transformations in Ti-Al-X alloys. The application of these new experimental techniques has revolutionized our old concept of phase stability. The rapid developments in this area owe much to innovations in instrumentation. The current spurt in research on the study of phase transformations in Ti-Al-X alloys has been triggered by opportunities and challenges, which continue to attract scientific interest. It is interesting to note that the theory of phase-transformations in Ti-Al-X alloys and its experimental verification stimulate each other. The study of phase transformations in Ti-Al-X alloys continues to absorb a large share of attention, as it has been a most active field of research in recent years. Despite the great success achieved in the past two decades in understanding phase trans-

formations in Ti-Al-X alloys, much remains unknown and the subject is therefore fascinating as well as promising. While preparing this paper, a fundamental approach to phase transformations in Ti-Al-X alloys has been followed to develop a few central ideas of microstructural stability. Analytical discussion led us to focus on various aspects of microstructural control in Ti-Al-X alloys. Emphasis has been placed on the provision of theoretical descriptions of various phenomena. An interesting microstructural feature, which appears to be unique to Ti-Al-X alloys, is the formation of lamellar structures. Proper control of microstructures provides improvement in tensile strength and creep resistance. Fracture resistance in these alloys stems from intrinsic and extrinsic toughening mechanisms, which have been handled with the help of appropriate experimental observations.

Titanium is one of those elements that develops attractive high temperature properties by suitable combination of alloying elements and proper heat treatment. Aluminium in particular is an inevitable constituent of such compositions. It imparts high strength, high temperature properties, and oxidation / corrosion properties at a low density. However, room temperature ductility remains a limitation to Ti systems. Multimetallic composition leads to variation in precipitation phenomena within either an equiax or lamellar microstructure for both wrought product and lamellar/ dendrites in as cast products.

Ordered B2-phase appears at high temperature in Ti-Al-X (X = Ta, Nb and Mo) system, which cannot be arrestable by rapid solidification processing. Massive ordering transformation on cooling from homogenization temperature has been reported in Ti-14Al-2Zr-3Sn-3Mo-0.5Si alloy, leading to substantial reduction of acicular α_2-particles by aging. Massive transformation is observed in Ti-45Al alloy containing Nb and Mn on quenching from 1623K. Phase transformation in Ti-48Al (at.-%) at different oxygen content upon quenching forms α-phase, refines lamella structure by nucleation of fine α_2 platelets, in addition to massive transformation up to a limit of 1.2 (at.-%). Above this limit of oxygen chemical ordering reaction dominates massive transformation.

Creep and high temperature tensile properties in the case of nitrogen doped system of Ti-48.5Al-1.5Mo (at.-%) alloy have been studied. Reduction in grain growth by Zener pinning effects leads to appreciable reduction in ductility. Continuous solid solution is detected with variable composition $(Ti_{1-x}, Nb_x)_3(Si_{1-y}, Al_y)$ (η) (a peritectoid) in Ti-Al-Si-Nb alloy at low Nb and Si content. On the other hand, ductility improves by Si partitioning among β_o, α_2, O-phase and silicides in an alloy of TiAl containing Nb. An ordered solid-state phase has been observed on quenching Ti-Al-C and Ti-Al-Nb-C alloys from 1523K. Reduction of wire drawing temperature by the addition of Mo to a shape memory alloy based on TiNi binary system lowers withdrawing stresses in relation to two-step phase transformation given by B2 (parent cubic phase) to R (rhombohedra phase) and further to B_{19}' (monoclinic)-phase. Super α_2-phase forms metastable B2-phase at interface by a single heat treatment step after forging and improves mechanical properties and ductility more than a two-step heat treatment after forging of Ti-25Al-10Nb-3V-1Mo alloy. Ellipsoid ω-phase displays four variants in the same growth direction in as aged condition in Ti-20 wt.-% Mo and Ti-14 wt.-% Mo. Improvement in creep rupture life has been reported by alloying β-phase stabilizers to TiAl in a $Ti_{52}Al_{48-x}M$ (where M = Fe, Cr, V, or Nb) system, so as to produce solid solution strengthening of γ-phases before the onset of B2-phase formation. Phase instability leads to softening both in the lamellar and granular phases. Phase stability and instability mechanisms play an important role in the high temperature performance of Ti-alloys. For example, the structure stability of Al_5Ti_3 and h-Al_2Ti in $L1_0$-TiAl formed in both as cast and/or as annealed has been reported. Microstructure of creep deformation in hard oriented Ti-48Al polysynthetically twinned crystal with lamella plates parallel to compression axis shows pseudo-twins. Rotational fault interfaces are less thermally stable than true twin γ/γ interfaces, but α_2/γ interface is more stable than γ/γ interfaces. In polysynthetically twinned single crystal of (γ-TiAl + α_2-Ti_3Al) lamellae, the plastic deformation is controlled by softer γ-TiAl phase as well as harder α_2-Ti_3Al phases. Polysynthetically twinned polycrystalline fully lamellar Ti-46Al (at.-%) after refining by solution treating at α-phase region and aging within (α_2 + γ) region produces ultra fine lamellae that lead to an exceptional tensile strength and unstable creep

resistance. Colony boundary resistance of fully lamellar binary microstructure of Ti-46Al prevents crack propagation with minimal accompanying damage at boundary to arrest crack. It also prevents multiple crack nucleation, ligament formation and failure of ligament, while within individual colonies crack propagates with minimal resistance. The room temperature strength properties of Ti-48Al-γ Ti aluminides become limited on increase of volume fraction of lamellar colony in comparison to duplex microstructure. Lamellar interfaces and domain orientation play a critical role in controlling the mechanism properties of TiAl based alloys. Alloying elements of lamellar TiAl alloy ($Ti_{48.55}Al_{47}Cr_2Nb_1Ta_{0.8}W_{0.2}Bo_{0.15}Si_{0.3}$ alloy) segregate at ledges in the crept microstructure. The amount of segregate varies on stress concentration and distortions in lattice by applied stress, so as to improve creep resistance. Creep in powder metallurgy alloy of Ti-47Al (+ Cr, Nb, Ta, W, Si) segregates micro-alloying elements at lamellar interfaces especially at ledges to interact with misfit and/or disorientation dislocations at interfaces to regard climb of dislocation, although large segregate (Nb, Ta, W) is effective in reduction while small segregate (Si) increases climb rate to dissolve α lath and coarsen γ-lamellae and subsequent decreases in creep resistance by a factor of 3-4.

Precipitation of $L2_1$-Ni_2TiAl Heusler phase from super saturated B2-TiNi matrix at 873-1073K has been utilized to develop high strength TiNi shape memory alloy. $B2/L2_1$ is a fully coherent two-phase microstructure. Heusler precipitate follows coarsening kinetics at 873K and growth kinetics at 1073K in the case of Al, Zr and Hf substitution for Ti, but follows one kinetic behavior at both temperatures when Ni is substituted by Pt and Pd. Using quantitative microstructures analysis, partitioning behavior of Hf, Pd, Pt and Zr has been established. Ti rich TiNi thin films with GP zones show a large transformation strain while thin films with Ti_2Ni precipitate show a relatively small transformation strain, because spherical Ti_2Ni precipitates impede shear deformation of martensite transformation. Precipitation of K_5 γ-ΓiAl in Ti-46Al-2Cr-3Nb-0.2W alloy increases high temperature resistance through refinement of interstitialcy (C and C + Si), whereas light element precipitates by nucleation and growth in the form of H-type carbides and ζ-type silicides at the expense of dissolving α_2-laths during aging. $Ti_{50}Pd_{43}Fe_7$, a shape memory alloy (SMA) under transmission electron microscope (TEM) shows the existence of type I, type II and compound twins. Compound twins cause lattice variant deformation in the region of 9R martensite, where type I and type II twins are responsible for lattice invariant shear in 9R martensite coexisting with 2H martensite. A twin is an important deformation mechanism of γ (TiAl). It is produced when a dislocation misfitting to the interface triggers at grain boundaries, so as to initiate an eigenstress field of twin nucleus. Elastic energy release from rapid twin development compensates interfacial and intrinsic dissipation energy. Under varying loads a discrete twin band is separated by periods of quasistatic growth of existing twins. When Shockley partial of matrix is activated, a type I twin intersection appears in preference to a type II twin intersection. A type II twin intersection is accomplished by a shear reshuffle process in TiAl alloys. Cooling rate variations of solution treated IMI 550 / Ti-4Al-4Mo-2Sn-0.5Si) alloy form orthorhombic martensite at higher temperature (1233K), while hexagonal martensite is formed at near high (1223K) temperature and renders parent phase stability below 1123K, where alloy partitioning at decreasing solutionising temperature produces chemical short range ordering in the parent phase.

ORDER-DISORDERED PHASE TRANSFORMATION

Studies of ordered phase (B2) formation in a Ti-Al-X (X = Ta, Nb or Mo) system using differential thermal analysis have been done /1/. Ti-33Al-17Ta alloy shows B2 phase stability up to 1478K. The solid states ordering of the B2-phase from the disordered bcc phase results in anti-phase boundaries (APBs). Similarly ordered reaction to form B2-phase exists up to 1414K for Ti-25Al-25Nb alloy and up to 1691K for Ti-25Al-25Mo alloy. Microstructural instability, high oxidation and poor high temperature strength retention of Ti-alloys restrict their application above 873K. The α_2-base intermetallic (Ti_3Al) appears to be intrinsically poor in ambient temperature toughness. Precipitation strengthening in the α_2-phase combines the advantages of both

disordered and ordered structure. It produces an improvement in elevated temperature properties. Precipitate in the α_2-phase acts as a barrier to dislocation motion above the temperatures of thermal activation of solutes and grain boundary sliding. Acicular α_2'-particles form along α/β-phase boundaries in Ti-14Al-2Zr-3Sn-3Mo-0.5Si alloy. On cooling of the alloy below ordering transformation temperature, massive α_2-phase transformation occurs, where lattice mismatch between the α- and the α_2-phases is very small, with a/c value close to that of pure α-Ti. Sn and Zr strongly favour the Al and Ti sub-lattice respectively of α_2-phases without any effects on the ordering reaction /2/. Acicular α_2-phase formation between the α and β-phase fields depends on the thermo mechanical history, fast ordering kinetics, capability at the phase boundaries and anisotropic diffusion of aluminium to the specific direction.

MASSIVE TRANSFORMATION

The ($\alpha \rightarrow \gamma_m$) massive transformation in TiAl alloys occurs when the alloy is cooled from the α-phase field at a faster rate to suppress ($\alpha 2+\gamma$) lamellar microstructure formation /3/. Susceptibility to undergoing massive transformation increases through the addition of Nb to binary Ti-45Al alloy. However, the reverse mechanism has been observed on increase of Mn in the system. The tendency of massive transformation is influenced by prior grain size and nucleation rate. Shifts in the C-curve for massive as well as ($\alpha \rightarrow \alpha+\gamma$) lamellar transformation to shorter time have also been observed by increasing Mn content. Heterogeneous nucleation at prior α-grain boundaries and growth by short-range transfer of atoms across incoherent interface takes place in massive transformation /3/. Oxygen inhibits massive transformation in Ti-48 Al at.% when its content is above the critical value of 1.2 at.-% /4/. Below the critical content the massive transformation prevails. Excess oxygen in γ_m-phase after massive transformation tends to reach α_1-plates formed within γ_m-structure. Oxygen promotes α_2 platelet precipitations. Oxygen also favors chemical ordering of α-phase. Quenching from (α + γ) dual phase field leads the chemical ordering. A first chemical ordering has been found ($\alpha \rightarrow \alpha_2$) at 1423K for commercial alloys. A second chemical ordering has been found ($\alpha \rightarrow \alpha_2$) at 1523 K for oxygen-doped Ti-48Al alloy containing 8000 at.ppm. The oxygen stabilizes α_2 against α-phase. Figure 1 shows the schematic CCT diagram of chemical ordering reaction ($\alpha \rightarrow \alpha_2$) before massive transformation at high oxygen content /5/.

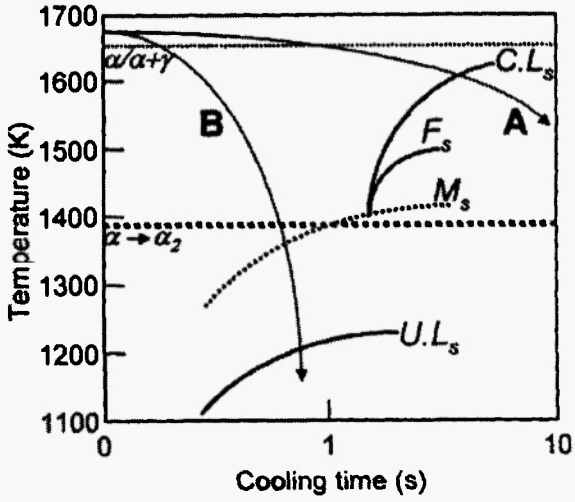

Fig. 1: Schematic CCT diagram of the Ti-48 at. % Al alloy significantly oxygen enriched, where CL_s = classical lamellar structure; F_s = Feathery structure; M_s = massive γ_m structure; and UL_s = ultra fine lamellar structure, A and B represents two cooling rates from the α single-phase field /4/.

ELEMENTAL PROPOSITIONS IN PHASE TRANSFORMATION

The importance of titanium and vanadium compounds in the form of nitrides, carbides and carbonitrides in the Ti-V-N system has been recognized, as these compounds lead to strengthening. Based on nitrogen content, two or three phases may be present. These are given by vanadium-rich, low-nitrogen, solid-solution phase of bcc crystalline, titanium-rich α-$(Ti,V)N_x$ phase (x~0.2) of hcp crystalline and an fcc nitride. Volume fraction of the fcc phase increases at the expense of the hcp phase with increasing nitrogen content. Titanium rich fcc nitride is a highly non-stoichiometric phase. Annealing at 1273 K changes the

cast structure rapidly /6/. A remarkable improvement in creep resistance of duplex microstructure and fully lamellar microstructure is observed with the addition of nitrogen in Ti-48.5Al-1.5Mo alloy. 1 at.-% nitrogen doped equiax and a fully lamellar alloy show better creep resistance. Solute and precipitation (p-phase) hardening result in increase of creep resistance, as shown in Fig. 2 /7/.

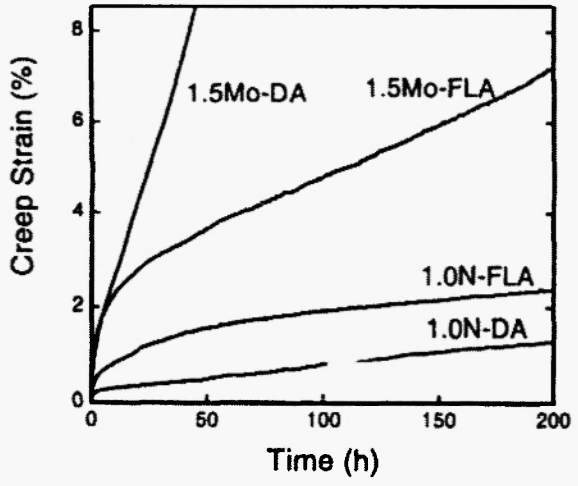

Fig. 2: Creep curve of the 1.5 Mo and 1.0 N alloy with the fully lamellar and duplex microstructure at 1073K, 200MPa and air environment /7/.

Varying α-phase distribution and morphology within metastable β-Ti alloys through different aging treatments offer a wide range of mechanical property combinations. The presence of bcc β-phase allows easier deformation during direct hot rolling deformation prior to aging treatment. Higher alloying does not precipitate α-phases and thus retains deformability even after multifold increment of tensile strength. Microstructural inhomogeneity after deformation in β-titanium alloy leads to a wide scatter of particles after aging. A narrow temperature range processing followed by a solution treatment reduces inhomogeneity. High solution temperatures first refine the grains and then coarsen them rapidly because of the absence of a second phase and thus facilitate further steps of processing and improvement of mechanical properties. The refining ability can be further improved if the as cast metal contains fine grains through controls over solidification mechanism. The effects of B, C and Si on the metastable Ti-15Mo based alloy have been studied /8/. As cast equiax grain formation is not possible, though dendrite solidification is promoted as compared to cellular. Silicon appears to be less effective under any condition of treatment to the microstructure. Lack of further phase transformation during cooling and narrow (solid + liquid) phase field in the Ti-Mo system inhibit refinement to fine equiax grains. The forging process refines grains to a large extent in the presence of boron and carbon. The presence of borides and carbides at grain boundaries produces Zener pinning effects to reduce grain coarsening during solution treatment. Borides and carbides increase cavitations after the processing step and reduce ductility by forming a fracture site at the boride particle and void nucleation around carbides. Therefore B and C do not improve properties by conventional routes /9/.

Participation of two α-phase versions in a phase diagram of the Ti-Si system has been studied in a ductile Ti matrix of a Ti-Al-Si-Nb system /10/. Structural characterization of a multi-component Ti-Si alloy system shows continuous solid solutions with variable compositions $(Ti_{1-x}, Nb_x)_3(Si_{1-y}Al_y)$ (η) ($0.05 < 0.07$, $10\text{-}3 \leq y \leq 0.02$). Under low aluminium content, the addition of Nb stabilizes this phase. Increasing aluminium content neutralizes the stabilizing effect of Nb and favours peritectoid reacting ($\beta + \alpha \rightarrow \eta$) and results in a [$\alpha + Ti_5Si_3$ (χ)] equilibrium. The unstable Ti_3Si is stabilized by Nb within iso-structural of Ti_3Si and Nb_3Si by ($\beta + \alpha \rightarrow \eta$) peritectoid. Nb loses the stabilizing effect and forms ($\alpha + z$),($\alpha_2 + z$) and ($\alpha + \beta + z + \eta$) when Al content exceeds 10%. Multi-component alloy systems improve the combination of properties of Ti-Al binary systems. The addition of Nb improves properties by β-phase stabilization. The existence of ternary orthorhombic phase designated by O-phase also appears when Nb content is greater than 11%. α_2-phase precipitation from β-phases during continuous cooling from high temperatures like welding or during heating of metastable β or β_o leads to attractable combination of properties. A further introduction of Si into the Ti-Al-Nb system increases ductility. In the Ti-Al-C system ($\beta \rightarrow \alpha + Ti_5Si_3$) eutectoid changes to ($\beta + Ti_5Si_3 \rightarrow \alpha$) peritectoid after the addition of α within the temperature range of 873-1273K. In the four-element system of Ti-Al-Nb-Si, the Si partitions to β-

phase in preference to α_2-phase and O-phase /11/. Alloying behavior, the microstructure and the high temperature tensile properties of the Nb added Ni_3 (Si, Ti) alloys have been studied. The solubility limit of the Nb element in the $L1_2$ Ni_3 (Si, Ti) phase at 1273K was 2.7%.

$D0_a$-type Ni_3Nb and $Ni_{12}Si_4TiNb_2$ compounds which were incoherent with the Li_2Ni_3 (Si, Ti) matrix have been identified. These second phases form when the solubility limits are exceeded. Strengthening over a wide range of temperatures, as well as improvement in the high temperature tensile elongation, have been observed by Nb-containing second phase dispersions in the $L1_2Ni_3$ (Si, Ti) phase matrix /12/. The development of TiAl alloys with reference to room temperature brittleness and high temperature oxidation requires the addition of β-phase stabilizers (Nb, V, W, etc.) or super α_2-formation (Ti-25Al-10Nb-3V-1Mo at.-%). Adding carbon into TiAl intermetallic with or without Nb at a different carbon percentage refines precipitate dispersion into the matrix. It increases ductility by slip dispersion. Five to 12% Nb alloying into α_2-based intermetallic consisting of 3% C produces β-phase and improves ductility /13/. Modification of intermetallics by carbon has been studied in Ti-Al-C ternary system /14/. It reveals the presence of Ti_3AlC (Phase-P) and Ti_2AlC (Phase-H) ternary carbides in titanium rich portions of the system. Studies have been done at 1523, 1323 and 1023K isotherm sections in a Ti-rich portion of Ti-Al-C system based on Ti_3Al and Ti Al. The existence of carbide phases such as TiC, Ti_3AlC (P-phase) and Ti_2AlC (H-phase) during solidification of (15Al-3C), (26Al- ≥ 0.5C) and (55Al-1C) alloys, respectively, has been reported.

An R- (rhombohedral) phase in the Ti-Ni system can be induced by the addition of Mo. Two-stage phase transformation in the Ti-Ni-Mo system can be described by transformation of the B2 (cubic) parent phase to the R-phase and transformation of the R-phase to B_{19}'-(monoclinic) phase /15/. The addition of Mo to Ti-Ni binary alloy facilitates wire drawing. Vacuum annealing treatment decreases the wire drawing stresses monotonically. During annealing treatment in air, the drawing stress decreases with rising annealing temperature up to 913K and then increases. Reduction in drawability of the wire results from thick oxide scale that forms on wire surfaces when optimum annealing temperature of 823K is exceeded for the alloy Ti-Ni-Mo. Room temperature brittleness and low fracture toughness have been studied on super alpha-2 alloy of the system Ti-25Al-10Nb-3V-1Mo /16/. Microstructures produced by different thermo-mechanical processing and heat treatment routes affect mechanical properties of the alloy. The best balance of room temperature ductility and elevated temperature properties is obtained from transformed β-phase microstructure that produces elongated plate-like α_2-phase. Room temperature ductility of Nb-rich super α_2 alloy is improved by direct aging at 1073K after forging. The deterioration in mechanical properties associated with interface O-phase is given in Table 1.

Table 1
Room temperature tensile properties of β field forged super alloy α_2 alloy /16/

Sample treatment	$YS_{0.2}$, (MN/m^2)	UTS, (MN/m^2)	El %
As forged	909	1081	2.82
	855	1009	1.65
Forged + aged at 1073K for 2 hrs	873	1123	3.30
	891	1123	3.45
Forged + solution treated at 1303K for 1 hr + aged at 1-73K for 2 hrs	880	1133	1.40
	810	1092	1.20

Either coherent precipitates or dislocation structure or chemical composition define the presence of R-phase in the TiNi system. Two types of thermo-elastic martensite transformation occur on cooling. The R-phase is useful for many industrial applications because of its small enthalpy of transformation and low temperature hysteresis. The sequence of transformation is: B2-parent phase → incommensurate (IC) → commensurate (R) → B19′ martensite. Modulated lattice relaxation or charge density wave explains the R-phase transformation /17/. The aging and refining of Ti-Mo alloys result in the appearance of ω-phases, which subsequently reduce ductility and increase strength. As quenched deformation bands of Ti-14 wt.-% Mo form via twinning, where the existence of ω particles shows longer size than those present in matrix /18/.

STABILITY OF PHASES IN TITANIUM ALLOYS

High temperature performances of γ-TiAl based alloys have been reported in which ordered B2-phase has been stabilized by the addition of alloy. Annealing within 973K and 1073K for 10,000 hours in an air furnace on Ti – 46.5 at.-% Al – 4at.-% (Cr, Nb, Ta, B) – 0.22 at.-% O reveals B2-phase transformations into a C14-Laves phase with the nominal composition of $(Cr, Al)_2$ (Nb, Ta, Ti). Non-thermodynamically formed phases during rolling may disappear afterwards or transform into stable phases during high temperature exposure /19/. Optimizations of mechanical properties of TiAl alloys through control of alloying and microstructure have been tried. The strong influence of chemical composition on mechanical properties originates from (i) solid solution strengthening (Cr, Mn, V, Nb, Fe, Mo, W, etc.) and (ii) precipitation strengthening (B, Si and C). Si increases creep and oxidation resistance, while B refines the microstructure of TiAl. Cr, V and Mn enhance the plasticity of TiAl. Oxidation resistance and elevated temperature strength improve with the addition of Nb. However, the appearance of B2-phase (Ti_2AlCr) in Ti-48Al-3Cr alloy reduces the strength and ductility. On the other hand, B2-phase in Ti-44Al-2Mo improves mechanical properties /20/. The addition of Fe, Cr, V and Nb in $Ti_{52}Al_{48-x}M$ alloy forms an Al-rich B2-phase. Increasing the content of Fe, Cr, V and Nb in the alloy increases solubility in the γ phase and generally decreases lattice parameter ratio c/a. A decrease in (α/α + γ transus) by V and Nb and a small effect of Cr on α/α + γ transus have been observed. $Ti_{52}Al_{48}$-0.5Fe, $Ti_{52}Al_{48}$-1.0Cr, $Ti_{52}Al_{48}$-2.0V and $Ti_{52}Al_{48}$-2.0Nb show a peak in yield strength at room temperature. $Ti_{52}Al_{48}$-0.5Fe, $Ti_{52}Al_{48}$-2.0Cr, $Ti_{52}Al_{48}$-2.0V and $Ti_{52}Al_{48}$-4Nb show a peak in yield strength at 1173K. The reported values are 360, 406, 495 and 503 MPa respectively. $Ti_{52}Al_{48}$-0.5Fe, $Ti_{52}Al_{48}$-1.0Cr, $Ti_{52}Al_{48}$-2.0V and $Ti_{52}Al_{48}$-4.0 Nb show the highest creep-rupture lives in ternary TiAl alloys under a condition of 1073K/240 MPa. Room temperature hardness and brittleness increment and elevated temperature softness and ductility decrement have rendered B2-phases under strict control. The B2-phase decreases the ductility at room temperature and tensile strength and creep resistance at high temperature. Thus, initial increment of Fe, Cr, V and Nb contents improves properties by solid solution strengthening of γ-alloy, whereas a further increase of the third element reduces properties by B2-phase stabilization. Cr improves ductility at room temperature, V increases tensile strength at room temperature and Nb improves tensile strength and creep resistance at high temperature (Table 2).

Table 2
Chromium equivalent and the tensile and creep rupture properties of TiAl /20/

Alloy	σ_b MPa (298K, Tension)	δ, Pct. (298K, Tension)	Creep life, h (1073K, 240 MPa)	[Cr]
Ti-46.5 Al-2V-2Cr-0.5Mo	525	1.0	47.4	3.75
Ti-46.5 Al-2V- 2Cr	623	1.5	111.8	3.0
Ti-46.5Al-1V-1.5Fe	354	0.5	53.5	3.5
Ti-46.5 Al-2Nb-2Cr-0.5Fe	499	0.9	15.5	3.67
Ti-47 Al-2Nb-2Cr	623	1.5	80.5	2.67
Ti-46.5Al-2.5V-1Cr	622	1.0	77.5	2.25

Softening and microstructural instability have been studied in Ti-46.5Al-2W-0.55Si system /21/. Annealing destabilizes the lamellar microstructure and forms a globular structure composed of γ-matrix, fairly equiaxed globules of B2-phase and remnant occasional phases of α_2 or Ti_5Si_3-particles. It has been shown that the decrease in strength is proportional to the initial volume fraction of B2-phases. The lamellar structure of Ti-rich Ti_3Al in TiAl as the second phase favors toughness and creep properties. Similar low-density inter-lamellar Al-rich TiAl phases produce greater oxidation resistance by forming Al_2O_3 scale. Next to the aluminium-rich side there exist superstructures of basic $L1_0$ TiAl. These are tetragonal phases of Al_5Ti_3, H-Al_2Ti and R-Al_2Ti. Long range ordered superstructures form by aluminium substitution in place of titanium in a TiAl structure. Antisite atoms compensate the deviation from stoichiometry. A large deviation forms superstructures of Al_5Ti_3 and H-Al_2Ti. Studies reported the existence of non-equilibrium phases below super saturation of TiAl /22/. It leads to

precipitation of phases of different composition more easily from TiAl matrix than equilibrium phase of R-Al_2Ti. H-Al_2Ti is a metastable phase up to 1473K and transforms slowly to produce R-Al_2Ti. Metastable Ti_5Al_3 decomposes and develops lamellar structure of TiAl and Al_5Ti_3 after coarsening of small precipitates in Ti-62 at.%Al alloy. A prospective light material, Ti-48Al PST, for high temperature structural applications such as automotive and airways engine components, has been developed /23/. Creep resistance is optimized in this system by designing microstructure that consists of TiAl (γ) and Ti_3Al (α_2) –phases. These TiAl alloys consist of a two-phase lamellar microstructure, a favorable composition for applications that requires superior fracture toughness and creep resistance. Using the available experimental information pertaining to the active slip systems, the deformation resistance hardening behavior of the two constitutive phases both in the single-crystalline and in polysynthetically twinned lamellar forms have been studied. The constitutive relations have been implemented in a vectorised user materials subroutine (VUMAT), which is a commercial finite element program Abaqus. The result suggests that the adopted crystal plasticity model and the parameters used have associated quite well for the observed room temperature deformation behavior of poly-synthetically twinned lamellar (γ-TiAl + α_2-Ti_3Al) single crystals /24/.

CHARACTERISTICS OF LAMELLAR STRUCTURES

Refinement of lamellar spacing in a fully lamellar fine-grained titanium aluminide is highly desirable for an improvement in tensile strength and creep resistance. Equiax grain boundaries (related to poly-crystals), domain boundaries (soft mode deformation) and lamellar boundaries improve strength as per the Hall-Petch equation /25/. Intrinsic and extrinsic toughening mechanisms in lamellar two phase TiAl/Ti_3Al (γ/α_2) alloy have been studied /26/. Intrinsic toughening arises from matrix slip and ductile phase blunting, whereas extrinsic toughening stems from crack deflection, ductile-phase bridging, shear ligament toughening, microcrack shielding. Fracture resistance of these alloys in monotonic loading stems from intact ligament bridging in the crack wake. The advancing cracks within the colony do not exhibit observable surface damage; instead, they are stopped by large lamellar twist misorientation.

Traverse cracks across boundaries originate from multiple microcrack nucleation in the new colony, the presence of bridging ligaments that subsequently rupture with accompanying plastic deformation. In the case of a stacked colony, translamellar fracture occurs by an energy intensive process. Formation of significant kink misorientation within stacks, crack splitting and finally rupture takes place by translamellar fracture. A mosaic of lamellar misorientation across colony boundaries is effective in arresting cracks by twisting, splitting and forcing an alternative high-energy fracture path to become operative in the individual colony, although deformation within an individual colony occurs readily. Yield stress, tensile elongation, fracture toughness and creep behavior in the case of directionally solidified (DS) TiAl alloys depend on lamellar orientation to loading axis and inter-lamellar spacing. A parallel orientation between lamellar and tensile direction shows a good combination of room temperature strength, ductility and toughness and creep strength.

The effect of lamellar structure on room temperature yield stress and micro-hardness of directionally solidified Ti-46Al-2W-0.5Si (at.-%) alloy has been studied where a constant volume fraction of hard Al_2O_3 particle reinforcement has been used in the invest cast turbine blade alloy /27/. Solutionising heat-treatment of DS ingots modifies microstructure and forms regular lamellar structure, elongated B2-particles, finer Ti_5Si_3-precipitates and constancy in volume fraction of Al_2O_3 particles (1.5 vol.-%). Dislocation motion impeded by aligned α_2-lamella results in dislocations pile up at α_2/γ-interfaces.

A decreasing (α_2 – α_2) inter-lamellar spacing increases the micro-hardness and YS of fully lamellar TiAl based alloy reinforced with constant volume fraction of Al_2O_3 particles according to the Hall-Petech equation. Grain sizes of these alloys have been the important factor in controlling ductility. Maximum ductility, yield stress and work hardening rate have been reported in 0.5 – 0.6-volume fraction of lamellar

constituent of the binary Ti-48Al alloy. Low ductility in these alloys stems from high work hardening rate and associated low mobility of dislocations. Deformation modes at room temperature for near γ-phase and complex structure are controlled by slip of unit dislocations and twinning; whereas in near and fully lamellar structure, the mode of deformation is controlled by twinning dictated by the Schmid factor /28, 29/.

Alloying by Si, C, Ta, W, Mn, V, Cr, Nb enhances creep resistance of TiAl alloys. The benefits of alloying arise from the segregation of elements at interfaces. W segregates at γ/α_2-interfaces, Cr, Mo and Ta segregate at pseudo-twin (60 deg. rotation) and 120 deg. rotational γ/γ-interfaces after off-stoichiometric microalloying. The motion of γ/α_2 ledges dissolves α_2 phase during creep deformation. Therefore ledges play an important role in reducing creep resistance by dissolving α_2-laths. Improvements in creep resistance by alloying bcc transition metal elements (Cr, Nb, Ta and W) and non-metallic elements (B and Si) have been observed to operate in $Ti_{48.55}$ $Al_{47}Cr_2Nb_1Ta_{0.8}W_{0.2}B_{0.15}Si_{0.3}$ alloy. Annealed alloy shows no segregation while crept micro-structure shows Si, Cr, Ta and W segregation at ledges and Si and W form slight segregation at α_2/γ-interface /30/.

The boundary segregation stabilizes α_2-phase and improves creep resistance by prevention of climb of partial dislocation from ledges. A decrease in lamellar spacing of fully lamellar TiAl alloys improves creep resistance by increasing the difficulty of shear in hard-oriented colonies and by decreasing the mobility of dislocations in soft-oriented colonies, without a concomitant loss in room temperature ductility. The addition of 0.3 – 1 at.-% nitrogen to the ternary Ti-48.5Al-1.5Mo increases both the tensile strength and the creep resistance. The effect of lamellar thickness, in relation to interstitial nitrogen content, on the mechanical properties of fully lamellar alloy has been reported /31/. Lamellar thickness increases by forming coarser Ti_2AlN particles when nitrogen content is increased beyond 0.3%, while below this value the stipulation width of lamellar structures reduces. An increase in aluminium concentration of single-phase α matrix leads to coarser Ti_2AlN at high temperature.

Ti-rich two phases [α_2 (Ti_3Al) + γ (TiAl)] alloys that contain a small amount of α_2-phase, a self-accommodating lamellar structure, have been studied. Typical lamellar structures consist of twin or pseudo-twin related γ ($L1_0$) orientation variants and α_2 ($D0_{19}$) phase. Multiphase and multi-domain lamellar structure develops a combination of properties. Deficits in the empirical heat-treatment schedule appear to be hindrances in the development of a specific lamellar structure. Strain-induced nucleation and elastic energy minimization lead to a higher population of twin-related domains over pseudo-twin related domains /32/. Escape and branching of unit height ledge into or from multiple height ledgesat interfacial boundaries of α_2/γ and γ/γ control the ledge creep mechanism for lamellar structure. Diffusion controlled ledge motion causes phase transformation as well as deformation. Transient creep behaviors at different strains, activation energy and stress exponent can be explained on the basis of diffusion controlled ledge mechanism. Creep properties of γ-phase containing refractory elements and fine lamellar structure are influenced by the interaction of alloy segregates with misfit and/or misorientation dislocations at the lamellar interface.

A decrease of creep resistance by 3-4 has been observed by addition of 0.3% Si, where as substitution of 1% Nb with 1% Ta and 0.2% Ta with 0.2% W has induced little effect. Dissolution of α_2-lamellae and coarsening of γ-lamellae at low and high stresses have been studied. Ledge site interfaces are zones of segregates of added element. Relations have been developed between the effect of alloying modification on creep at the macro scale and interaction of alloy segregates with misfit and/or misorientation dislocations at the atomic scale. While such interaction is facilitated in small segregates (Si), it is retarded in case of larger segregates (Nb, Ta, W). The activation energy for creep is related to the rate controlling diffusion process. At high stresses the bottom ledge C in Figure 3 can escape by the glide of the associated misfit dislocation. To complete this escape process, the misorientation dislocation, which is also associated with the escaping ledge, has to climb, and the misfit dislocation next to ledge (M) has to advance to the newly created terrace by climb /33-35/.

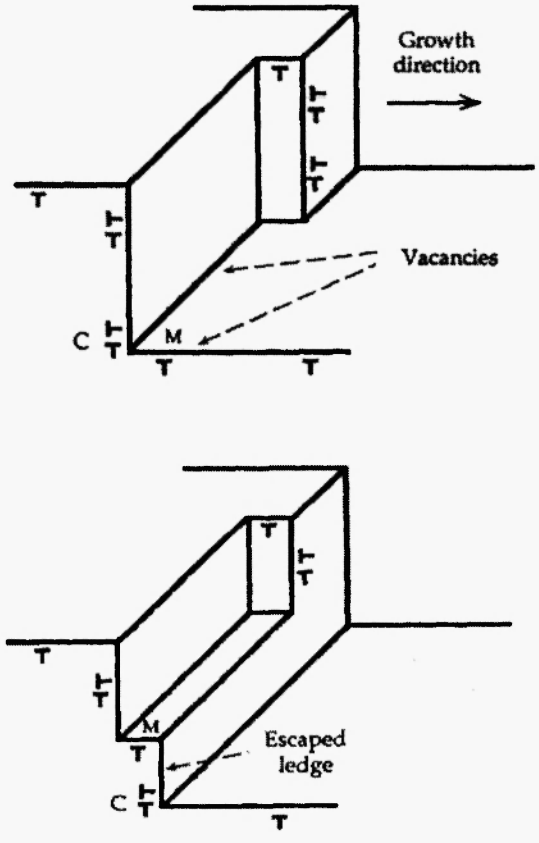

Fig. 3: Ledge motion by escaping of a unit ledge C (high stress state) /33/.

PRECIPITATION MECHANISM AND PROPERTIES

TiNi alloy with B2-structure and nickel content above 50.5 at. -% decomposes on aging below 1073K when initial state has been as quench from a high temperature. Initial break down appears to be a mixture of TiNi and Ti_3Ni_4-phases from an over-saturated B2-phase. R3 space group of rhombohedra identity is referred to as Ti_3Ni_4-precipitate or X-phase or unclear $Ti_{11}Ni_{14}$-phase. Lattice parameter of B2-structure is smaller than over-saturated TiNi phases. 3% crystal lattice mismatch leads to formation of internal stress to strengthen matrix and all round shape memory. In cases of low bulk defect density, Ti_3Ni_4 forms at grain boundaries and adjacent regions. Aging within 673K to 1173K produces precipitation of Ti_3Ni_4. Increasing temperature of aging reduces defect density and affects the process of precipitation. Reaction rate constant varies with annealing temperature, although precipitation mechanism remains the same. Annealing improves yield strength of a metal containing coherent Ti_3Ni_4 precipitates. Precipitate distribution does not affect the change in properties /36/. Using transmission and analytical electron microscope (TEM/AEM) and 3D atom probe microscopy (3DAP) in Ni-Ti-Al and Ni-Ti-Al-X (X = Hf, Pd, Pt, Zr) alloys, studies have done on the precipitation of $L1_0$-Ni_2TiAl phase from a supersaturated B2-TiNi matrix at 873K and 1073K /37/. Transmission electron microscopy (TEM), analytical electron microscopy (AEM) and three dimensional atom-probe (3DAP) microscopy in Ni-Ti-Al and Ni-Ti-Al-X (X = Hf and Zr) alloys have been used to study precipitation reaction in Heusler phase ($L2_1$: Ni_2TiAl) from a supersaturated B2 (TiNi-based) matrix at 873K and 1073K /38/.

Ti_2Ni precipitates disturb or impede the growth of martensite plates as they reduce the output of transformation strain during thermo mechanical cycling. GP zones do not affect growth of martensite plates during transformation or mechanical twinning shear. Therefore, they can be deformed elastically or can obtain a large shape recovery strain /39/. High temperature creep resistance improves by interstitial additions and precipitation hardening in fully lamellar gamma TiAl. Remarkable improvements of creep resistance after reinforcement with C or (C + Si) addition and aging have been reported in the alloy system K_5 (Ti-46Al-2Cr-3Nb-0.2W). Precipitation strengthening effects of B2-particles, ζ-type silicides and H-type carbide precipitation delineating γ/γ interfaces have been recommended for creep strengthening of K_5SC alloys. Using detailed electron microscopy involving high resolution imaging techniques and in –situ heating studies, the creep deformation of fully lamellar K_5 (S-C) type alloys in aged conditions have been studied. Strengthening of lamellar structure stems from the presence and relative distribution of these particles. Nucleation and growth of carbides and silicide precipitates at the expense of dissolving α_2-laths during aging depend on the nature of the light element precipitation process /40/. Ductility and toughness at room temperature are improved by the addition of the third element (V, Cr, Mn, Nb, Zr, Ta, Mo and W) into the TiAl system. Additions of Si into

TiAl alloy by powder metallurgy route introduce round Ti_5Si_3 particles and Ti_5Si_3 whiskers by ingot metallurgy. Ti_5Si_3 particles are heterogeneous precipitation products. Orientation relation and character of Ti_5Si_3/γ-interface have been studied /41/. Needle shaped particles precipitate at γ/γ-boundaries after addition of Cr and V in the system. Incoherent interface orientation exists between γ and Ti_5Si_3-phase in Si bearing TiAl alloy having polygonal / needle like shape (type I) and semi coherent interface orientation between γ and Ti_5Si_3-phase.

TWINS FORMATION IN ALLOYS OF TITANIUM

TEM investigation of 9R martensite in $Ti_{50}Pd_{43}Fe_7$ shape memory alloy shows in four twinning modes and two types of compound twins. The former two types are considered to be lattice invariant shear in 9R martensite. The gradual and random curvature with strain contrast reveals boundary of edge-on-state A: B type pair or irrational nature of type II twin boundary /42/. Titanium aluminide releases strain energy by shear transformation, which is triggered by dislocations at the grain boundaries. This is a different mechanism to that of twin band formation from twin nucleus /43/. Empirical three-stage stress-strain curves of Ti-Ni martensite polycrystal have been used for microstructural modifications. The first stage refersto the $<011>_{B19'}$ type II twin, recognized as a lattice invariant shear, and the formation of $(100)_{B19'}$ compound twin, where the rearrangement and coalescence of martensite variant take place concurrently. The second and third stages refer to the deformation by slip and twinning including compound twins. A consistent explanation of the relationship between deformed martensite and reverse transformed parent phases exists for both systems /44/. Deformation mechanisms include crystallographic slip and mechanical twinning in addition to elastic deformation. These two mechanisms produce shear deformation. Twinning results in a homogeneous shear that restores lattice in a new orientation. Thus orientation relations between twinned and untwinned region and atomic movement described by crystal element control the magnitude of twinning shear. Twin lamellae form on deformation in the form of narrow bands. The magnitude of deformation decides the thickness and separation of twin lamellae. A certain amount of resolved shear stress triggers both mechanisms. The formation of discrete twin bands based on energy criterion of stability of equilibrium can be predicted. The twin bands undergo uncontrolled rapid development as a result of release in elastic energy. Twin band thickness and critical resolved shear stress have been calculated by a compact analytical formula /45/.

Twinning is an important deformation mode in γ-TiAl. Alloying element and deformation temperature activate twinning. Twins impinge on grain boundaries and γ-α_2 interfaces (fully lamellar structure) as well as intersecting each other to activate multiple twinning systems provided these twins consist of nonparallel shear vectors. Based on the direction of the intersection line between barrier twin and incident twin, the two crystallographically non-equivalent types of twin intersections in an ordered tetragonal structure ($L1_0$) of the TiAl system have been observed. Deformation has been related to the appearances of type I and type II twin intersection. Type I twin intersection appears if the Shockley partial of Burgers vector in matrix is activated. Otherwise type II intersection appears. The proportion of appearance of type I and type II has been in the ratio of 1:2. Another mechanism refers to the shear-reshuffle mechanism of type II twin intersection by straight penetration /46/.

PROPERTIES OF MARTENSITE MICROSTRUCTURE

Methods of optimizing strength and fracture-toughness performance of (α - β) titanium alloy through variations in solution treatment temperature, cooling rate and aging temperature/times are in the developing stage. A beneficial influence on fracture toughness behavior of (α - β) alloy IMI 550 (Ti-4Al-4Mo-2Sn-0.5Si) is observed on an increase in solution treatment temperature and cooling rate. Super-plastic forming (SPF) capabilities have been higher in the case of IMI 550 than Ti-6Al-4V. In order to achieve acceptable

strength levels post SPF solution treatment is necessary in aged super-plastically formed and cooled components /47/. Chemical short range ordering (CSRO) in the high temperature β-phase due to a declining solution treating temperature has been observed. The island phase's parent crystal lattice consists of martensite. Misfit variants of crystal lattice between differently oriented islands of martensite and to that of parent phases have been observed.

A direct method to study crystallography of martensite transformation and its application to TiNi has been proposed /48/. Morphological differences between R-phases in TiNi have been observed and well explained. Shear assisted martensitic transformation has been established based on crystal plasticity, crystallography, thermodynamics, kinetics and statistics /49/. The essential features of stress assisted martensite transformation include (i) activation of nuclei of lower potency, (ii) formation of thin martensite plate, (iii) resistance of parent phase to martensite phase growth, (iv) the plate size decreases and the average plate aspect ratio increases with increasing extent of transformation. Equivalent stress-equivalent strain curves during stress-assisted martensite transformation under different stress and strain states in a polycrystalline Ti-10V-2Fe-3Al (wt. -%) alloy have been analyzed by implementing the commercial finite element code ABAQUS/standard. The applied stress state controls the equivalent stress—equivalent strain curves. Improved macroscopic strain states have primarily controlled the texture in the transformed Ti-10V-2Fe-3Al /50-52/.

CONCLUSION

Depending upon the structures titanium alloys have been classified as all alpha, alpha and beta and all beta. All alpha alloys are not responsive to heat treatment. The alpha-beta alloys are heat-treatable and possess good ductility. Beta alloys have relatively low ductility comparable to other alloys. Alpha-beta alloys are age-hardenable. Alpha alloys in general have highest strength at temperatures in the range 588-868K and possess the best resistance to oxidation in this temperature range. Their room temperature strength is not as good as the alpha-beta alloys. Addition of oxygen, nitrogen and aluminium raises transformation temperature. The stabilizing effect of aluminium on the alpha phase promotes stability at high temperature, which makes aluminium an important addition in many of the titanium alloys. The alloying elements such as iron, manganese, chromium, molybdenum, vanadium, columbium and tantalum stabilize beta phase and thus decrease alpha-beta transformation temperature. Addition of columbium and tantalum improves strength and prevents embrittlement. Nickel, copper and silicon are active eutectoid formers, while manganese, chromium and iron are sluggish in the formation of a eutectoid. Zirconium and tin are soluble in both the alpha and beta structures. A critical role in the design and development of TiAl is played by (a) lamellar interfaces, (b) domain orientation, (c) volume fraction of lamellar colony in a duplex alloy, (d) hardness variation between lamellar colony with reference to composition, (e) refining of lamellar colony in poly-crystals and (f) energy difference between boundary and grain of a binary lamellar alloy. Interface, invariant line strains, twin bands, high temperature dislocation assistance, tendency of lath dissolution with interstitials, phase invariant and orientation and partitioning behavior of alloying elements in a super saturated solid solution are some important factors which deserve attention.

The favorable properties of titanium alloys are lighter density, high strength, high specific strength and modulus, good high temperature strength retention properties, outstanding mechanical properties in the form of shape memory alloys and high temperature ductility of duplex alloys.

REFERENCES

1. K. Das and S. Das: *J. Mater. Sci.*, **38**, (19), 3995-4002 (2003).
2. A.J. Huang, G.P. Li, Y.L. Hao and R. Yang: *Acta Mater.*, **49**, (16), 4039-4952 (2003).
3. U. Prasad and M.C. Chaturvedi: *Metall. and Mater. Trans.*, **34A**, (10), 2053-2066 (2003).
4. W. Lefebvre, A. Loiseau and A. Menand: *Metall. and Mater. Trans.*, **34A**, (10), 2067-2075 (2003).
5. J.L. Quzi, O.N. Senkov, J. Rahim, A. Gene and

F.H.(Sam) Froes: *Metall. and Mater. Trans.*, **32A**, (10), 2453-2463 (2003).
6. A. Kroupa, J. Bursik, M. Svoboda, J.K. Chen and G.C. Weatherly: *Mater. Sci. and Technol.*, **18**, (1), 13-20 (2002).
7. Ju Hwan Yun, Han Seo Cho, Soo Woo Nam, Dang Moon Wee and Myung Hoon Oh: *J. Mater. Sci.*, **35**, (18), 4533-4537 (2000).
8. L.H. Chen, P.A. Blenkinsop and I.P. Jones: *Mater. Sci. and Technol.*, **17**, (5), 573-580 (2001).
9. Y.H. Wen, Y. Wang, L.A. Bendersky and L.Q. Chen: *Acta Mater.*, **48**, (16), 4125-4135 (2000).
10. N. Antonova, S.A. Firstov and D.B. Miracle: *Acta Mater.*, **51**, (11), 3095-3107 (2003).
11. D. Arrel, H.M. Flower and D.R.F.West: *Mater. Sci. and Technol.*, **12**, (8), 617-622 (1996).
12. T. Takasugi and M. Yoshida: *J. Mater. Sci.*, **36**, (3), 643-651 (2001).
13. G. Cam, H.M. Flower and B.R.F. West: *Mater. Sci and Technol.*, **7**, (7), 587-591 (1991).
14. G. Cam, H.M. Flower and D.R.F. West: *Mater. Sci. and Technol.*, **7**, (6), 505-511 (1991).
15. Tae-Hyun Nam, Dae-Won Chung, Jung-Pil Noh and Hce-Woo Lee: *J. Mater. Sci.*, **36**, (17), 4181-4188 (2001).
16. C. Huang, T.A. Dean and M.H. Loretto: *Mater. Sci. and Technol.*, **11**, (2), 143-149 (1995).
17. Danuta Stroz: *Scripta Mater.*, **47**, (6), 663-669 (2002).
18. E. Sukedai, H. Hashimoto, M. Hida and H. Mabuchi: *Mater. Sci. and Technol.*, **8**, (1), 3-9 (2001).
19. M. Beschliesser, H. Clemens, H. Kestler and F. Jeglitsch: *Scripta Mater.*, **49**, (4), 279-284 (2003).
20. Fu-Sheng Sun, Chen-Xiao Cao, Seung-Eon Kim, Yong-Tai Lee and Ming-Gao Yan: *Metall. and Mater. Trans.*, **32A**, (7), 1573-1589 (2001).
21. M.A. Munoz-Morris, I. Gil. Fernandez and D.G. Morris: *Scripta Mater.*, **46**, (8), 617-622 (2002).
22. F. Stein, L.C. Zhang, G. Sauthoff and M. Palm: *Acta Mater.*, **49**, (15), 2919-2932 (2001).
23. H.Y.Kim and K. Maruyama: *Acta Mater.*, **51**, (8), 2191-2204 (2003).
24. M. Grujicic and S. Batchu: *J. Mater. Sci.*, **36**, (12), 2851-2863 (2001).
25. C.J. Boehlert, D.M. Dimiduk and K.J. Hemker: *Scripta Mater.*, **46**, (4), 259-267 (2002).
26. P. Wang, N. Bhate, K.S. Chan and K.S. Kumar: *Acta Mater.*, **51**, (6), 1573-1591 (2003).
27. J. Lapin: *J. Mater. Sci.* letter, **22**, (10), 747-749 (2003).
28. G. Babu Viswanathan, Michel J. Mills and Vijoy K. Vasudevan: *Metall. and Mater. Trans.*, **34A**, (10), 2113-2127 (2003).
29. S.H. Chen, G. Schumacher, D. Mukherjee, G. Frohberg and R.P. Wahi: *Scripta Mater.*, **47**, (11), 757-762 (2002).
30. X.W. Du, J.N. Wang and J. Zhu: *Scripta Mater.*, **45**, (1), 19-24 (2001).
31. C.Y. Nam, M.H. Oh, K.S. Kumar and D.M. Wee: *Scripta Mater.*, **46**, (6), 441-446 (2002).
32. Y.H. Wen, L.Q. Chen, P.M. Hazzledine and Y. Wang: *Acta Mater.*, **49**, (12), 2341-2353 (2001).
33. J.N. Wang, J. Zhu, J.S. Wu and X.W. Du: *Acta Mater.*, **50**, (6), 1307-1318 (2002).
34. G.H. Guo, G.J. Shen, J.M. Liu, Z.G. Liu and W, Skrotzki: *Scripta Mater.*, **49**, (9), 797-802 (2003).
35. S.V. Divinski, F. Hisker, A. Bartels and Chr. Herzig: *Scripta Mater.*, **45**, (2), 161-167 (2001).
36. P. Filip and K. Mazanee: *Scripta Mater.*, **45**, (6), 701-707 (2001).
37. J. Jung, G. Ghosh and G.B. Olson: *Acta. Mater.*, **51**, (20), 6341-6357 (2001).
38. J. Jung, G. Ghosh, D. Isheim and G.B. Olson: *Metall. and Mater. Trans.*, **34A**, (6), 1224-1235 (2003).
39. J.X. Zhang, M. Sato and A. Ishida: *Acta Mater.*, **51**, (11), 3121-3130 (2003).
40. M. Karadge, Y.W. Kim and P.I. Gouma: *Metall. and Mater. Trans.*, **34A**, (10), 2129-2138 (2003).
41. F.S. Sun, S.E. Kim, C.X. Cao, Y.T. Lee and M.G. Yan: *Scripta Mater.*, **45**, (4), 383-389 (2001).
42. S. Ii, M. Nishida and T. Hara: *Scripta Mater.*, **46**, (7), 549-554 (2002).
43. F.D. Fischer, F. Appel and H. Clemens: *Acta Mater.*, **51**, (5), 1249-1260 (2003).
44. S. Ii, K. Yamauchi, Y. Maruhashi and M. Nishida: *Scripta Mater.*, **49**, (7), 723-727 (2003).
45. H. Petryk, F.D. Fischer, W. Marketz, H. Clemens and F. Appel: *Metall. and Mater. Trans.*, **34A**, (12), 2827-2836 (2001).
46. J.X. Zhang and H.Q. Ye: *Scripta Mater.*, **45**, (2),

133-138 (2001).
47. K.K. Kharia and H.J. Rack: *Metall. and Mater. Trans.*, **32A**, (3A), 671-679 (2001).
48. Yongmei M. Jin and George J. Weng: *Acta Mater.*, **50**, (11), 2967-2987 (2002).
49. M. Grujicic and Y. Zhang: *J. Mater. Sci.*, **35**, (18), 4635-4647 (2000).
50. K. Otsuka, X. Reu and T. Takeda: *Scripta Mater.*, **45**, (2), 145-152 (2001).
51. S.H. Kim, M.H. Oh and D.M. Wee: *Metall. and Mater. Trans.*, **34A**, (10), 2089-2095 (2003).
52. L. Daroczi, D.L. Beke, C. Lexcellent and V. Mertinger: *Philos. Mag.*, **82**, (1), 105-120 (2002).